ACS APPLIED MATERIALS & INTERFACES

www.acsami.org

Research Article

Triphenylene-Based Emitters with Hybridized Local and Charge-Transfer Characteristics for Efficient Nondoped Blue OLEDs with a Narrowband Emission and a Small Efficiency Roll-Off

Futong Liu, Gongyi Cao, Zijun Feng, Zhuang Cheng, Yan Yan, Yangze Xu, Yixuan Jiang, Yulei Chang, Ying Lv, and Ping Lu*

Cite This: *ACS Appl. Mater. Interfaces* 2023, 15, 47307−47316

Read Online

ACCESS | Metrics & More | Article Recommendations | Supporting Information

ABSTRACT: Developing high-efficiency nondoped blue organic light-emitting diodes (OLEDs) with high color purity and low-efficiency roll-off is vital for display and lighting applications. Herein, we developed two asymmetric D-π−A blue emitters, PIAnTP and PyIAnTP, in which triphenylene is first utilized as a functional acceptor. The relatively weak charge transfer (CT) properties, rigid molecular structures, and multiple supramolecular interactions in PIAnTP and PyIAnTP can significantly enhance the fluorescence efficiency and suppress the structural relaxations to obtain a narrowband blue emission. The photophysical experiments and theoretical simulations reveal that they both exhibit a typical hybridized local and charge-transfer (HLCT) excited state and achieve high external quantum efficiency (EQE) via a "hot exciton" channel. As a result, PIAnTP- and PyIAnTP-based nondoped devices realize blue emission at 456 and 464 nm, corresponding to CIE coordinates of (0.16, 0.14) and (0.16, 0.19), narrow full width at half-maximums of 52 and 60 nm, and the high EQEs of 8.36 and 8.69%, respectively. More importantly, the PIAnTP- and PyIAnTP-based nondoped devices show small EQE roll-offs of only 5.9 and 2.4% at 1000 cd m^{-2}, respectively. These results signify an advance in designing a highly efficient blue emitter for nondoped OLEDs.

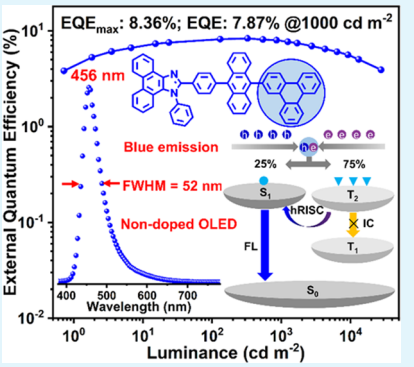

KEYWORDS: *nondoped devices, low-efficiency roll-off, narrow emission, hot exciton mechanism, blue OLEDs*

INTRODUCTION

Nowadays, organic light-emitting diodes (OLEDs) show high potential in panchromatic information display and lighting technologies owing to their advantages such as flat emission, low power consumption, good flexibility, etc.[1−4] Efficient blue emitters with high color purity (narrow emission spectrum) are the current concerns in commercialization OLEDs because they can widen the color gamut and reduce the energy consumption in ultrahigh-definition displays.[5−7] However, the development of blue emitters is relatively poor as compared to green- and red-emissive emitters because of their intrinsically wide band gap, high charge-injection barrier, and unbalanced charge mobility. In recent years, numerous blue phosphorescent materials[8−10] and thermally activated delayed fluorescence (TADF) materials[4,11−16] have attracted much attention because they can realize high electroluminescence (EL) efficiencies by harvesting both singlet and triplet excitons, but they always suffer from rapid efficiency roll-offs at high brightness due to the triplet−triplet annihilation (TTA) and have to be doped into suitable host materials to inhibit the accumulation of triplet excitons. Currently, the hybridized local and charge-transfer (HLCT) state has been reported as a favorable design strategy for high-performance blue materials, which can achieve high exciton utilization efficiency (EUE) by electron-to-photon conversion via the "hot exciton" route.[17−22] More importantly, the HLCT emitters harvest triplet excitons through a fast high-lying reversed intersystem crossing (hRISC) process, which can avoid the accumulation of triplet excitons and suppress the efficiency roll-offs at high luminance, laying the foundation for the preparation of a nondoped device.

In addition to the limitation of the spin statistics rule, the full width at half-maximum (FWHM) of the blue emitter, which determines the color purity of corresponding OLEDs, is another important issue for realizing an ultimate wide color gamut in next-generation ultrahigh-definition displays.[23,24] The strong charge-transfer (CT) characteristics in fluorescent materials usually cause relatively large structural relaxation of excited state molecule configuration, and unavoidably result in the broadband emission spectra with a typical FWHM of over 70 nm.[25] Despite recently the emerging multiresonance TADF

Received: June 30, 2023
Accepted: September 14, 2023
Published: September 26, 2023

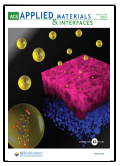

Downloaded via CHANGCHUN INST OMP on May 16, 2024 at 03:22:27 (UTC).
See https://pubs.acs.org/sharingguidelines for options on how to legitimately share published articles.

ACS Publications

© 2023 American Chemical Society

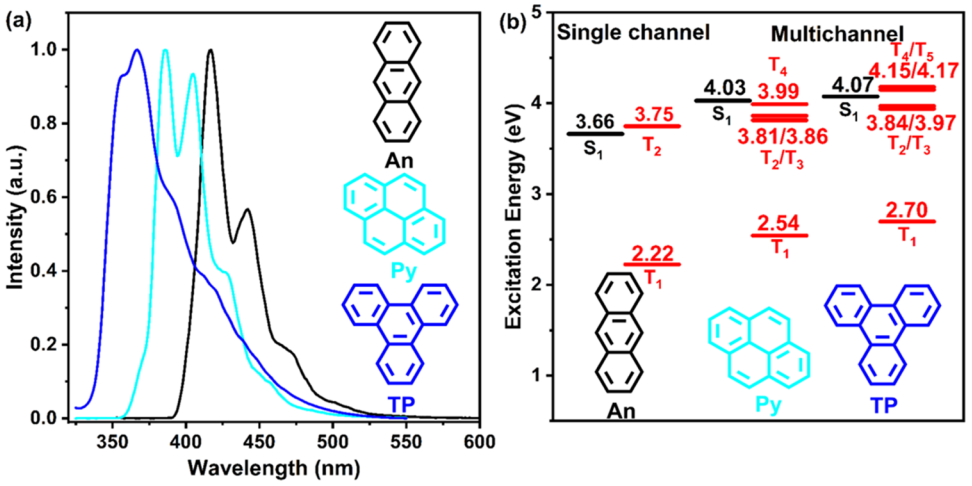

Figure 1. (a) Solution PL spectra and molecular structures. (b) Energy-level diagram of the calculated singlet and the triplet excited states for blue fluorescence PAHs (anthracene, pyrene, and triphenylene).

Scheme 1. Synthetic Routes and Chemical Structures of PIAnTP and PyIAnTP

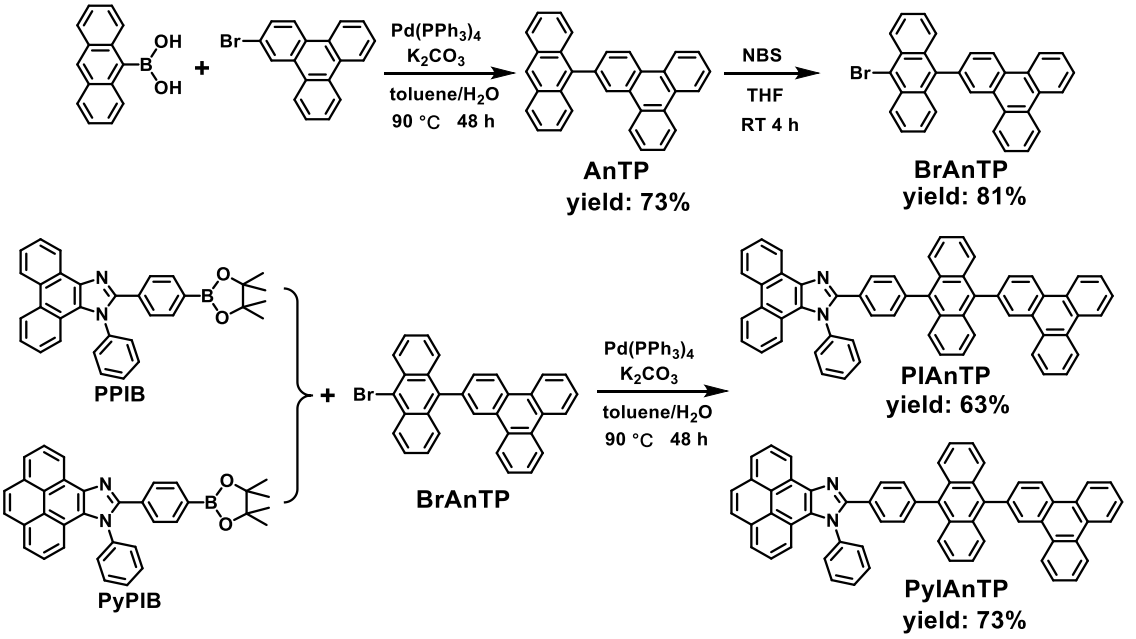

(MR-TADF) materials overcome the deficiency of color purity in conventional OLEDs to a great extent, they suffer from similar problems of severe efficiency roll-offs in doped OLEDs.[26−33]

In general, π-conjugated polycyclic aromatic hydrocarbons (PAHs) can serve as the desired skeleton for blue emitters owing to the relatively wide energy gaps (3.0−4.0 eV) and stable rigid structure, which are helpful in enhancing the photoluminescence quantum yields (PLQYs) and suppress the structural deformation.[34−36] A large number of PAH-based blue "hot exciton" compounds have been designed and synthesized.[22,37−40] Triphenylene (TP), a classical disk-shaped chromophore, has aroused extensive research interest recently because of its stiff planar structure, relatively weak electron-withdrawing capacity, and outstanding thermal and chemical stability.[41−44] Compared to other PAHs, TP shows bluer emission (λ_{em} = 367 nm) than that of anthracene and pyrene (Figure 1a). Moreover, TP also possesses a reasonable energy-level arrangement suitable for the multichannel hRISC process (Figure 1b).[39] Therefore, TP shows great potential in developing high-performance "hot exciton" blue materials.

The imidazole chromophore generally exhibits intrinsic bipolar properties derived from two nitrogen atoms with different bonding modes, which shows weak electron-withdrawing properties when linked to a stronger donor but can also serve as a weak electron donor when connected to the neutral group.[45−47] Herein, TP is first adopted to construct blue emitters as the acceptor moiety, while phenanthroimidazole (PI) and pyrenoimidazole (PyI) are chosen as the donors because of their planar rigid skeletons, high PLQYs, and bipolar transport abilities. In addition, anthracene with a large conjugated plane acts as the π bridge between donor and acceptor to finely regulate the local excited (LE) components and construct a weak CT excited state.[48−50] Two twisted D-π−A-type blue materials, PIAnTP and PyIAnTP, based on the asymmetric periphery enveloping strategy, are successfully

https://doi.org/10.1021/acsami.3c09433
ACS Appl. Mater. Interfaces 2023, 15, 47307−47316

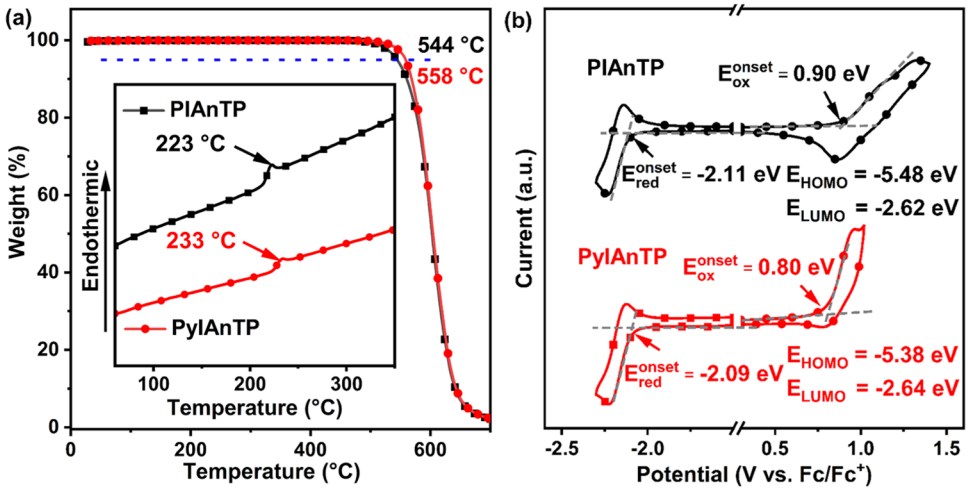

Figure 2. (a) TGA and DSC curves of PIAnTP and PyIAnTP. (b) CV curves of PIAnTP and PyIAnTP.

Table 1. Photophysical and Electrochemical Properties of PIAnTP and PyIAnTP

compound	$\lambda_{max,abs}$ [a] (nm)	λ_{max}/PLQY[a] (nm)	λ_{max}/PLQY[b] (nm)	E_g [a] (eV)	ΔE_{ST} [c] (eV)	HOMO/LUMO[d] (eV)
PIAnTP	308, 361, 376, 397	439/0.83	455/0.61	2.95	0.97	−5.48/−2.62
PyIAnTP	339, 359, 375, 385, 396	443/0.86	462/0.69	2.94	0.95	−5.38/−2.64

[a]Measured in THF at room temperature. [b]Measured in neat films at room temperature. [c]Measured in THF at 77 K. [d]Determined by CV.

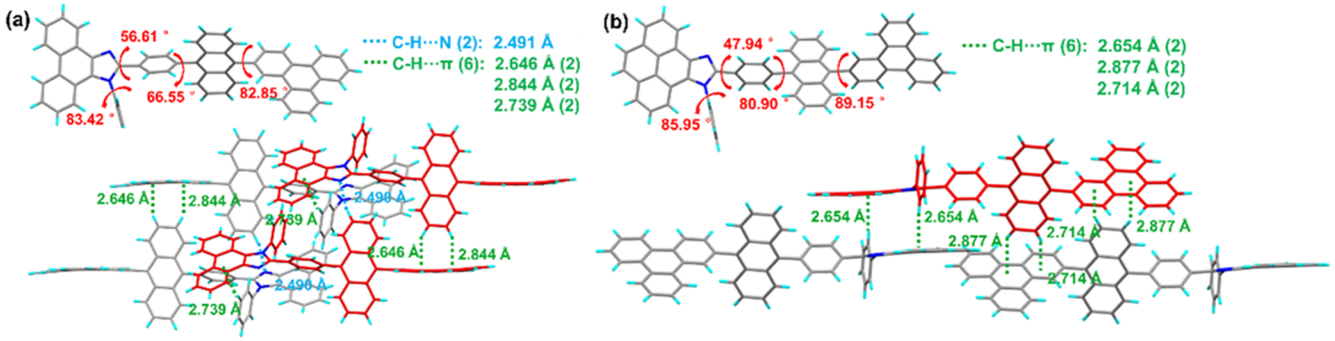

Figure 3. Single-crystal structures and packing motifs of (a) PIAnTP (CCDC 2266220) and (b) PyIAnTP (CCDC 2266221) in crystals.

synthesized. The rigid planar conformation, the multiple supramolecular interactions, and the relatively weak CT components in PIAnTP and PyIAnTP can lock the molecular conformation to induce efficient radiative transition and simultaneously suppress the structural deformation and vibronic couplings in favor of a narrow emission spectrum. As expected, the corresponding OLEDs based on PIAnTP and PyIAnTP both display pure blue emission with a small FWHM of 52 and 60 nm, Commission Internationale de L'Eclairage (CIE) coordinates of (0.16, 0.14) and (0.16, 0.19), maximum luminance (L_{max}) of 27 745 and 38 585 cd m^{-2}, and maximum external quantum efficiencies (EQE_{max}) of 8.36 and 8.69%, respectively. More importantly, the high-level EQEs of 7.87 and 8.48% are still maintained in the PIAnTP- and PyIAnTP-based devices at the luminescence of 1000 cd m^{-2}, showing small efficiency roll-offs. Crucially, this is the first example of the highly efficient TP-containing blue emitter exhibiting a "hot exciton" characteristic.

RESULTS AND DISCUSSION

Synthesis and Characterization. The syntheses of PIAnTP and PyIAnTP are illustrated in Scheme 1. PPIB and PyPIB were synthesized according to the previous literature.[51] AnTP was achieved by the Suzuki coupling reaction between 9-anthraceneboronic acid and 2-bromotriphenylene, which was brominated to obtain the intermediate BrAnTP. Then, the Suzuki coupling reactions between BrAnTP and respective boronized products of PPIB and PyPIB were performed to obtain the target molecules of PIAnTP and PyIAnTP with good yields. PIAnTP and PyIAnTP were purified with column chromatography and confirmed by nuclear magnetic resonance (NMR), mass spectrometry, and single-crystal diffractions. The synthetic details are summarized in the Supporting Information.

Thermal Properties and Electrochemical Properties. The thermal properties of PIAnTP and PyIAnTP were evaluated before the fabrication of OLEDs. As shown in Figure 2, the temperatures of 5% mass loss (T_d) for PIAnTP and PyIAnTP were as high as 544 and 558 °C, respectively. The differential scanning calorimetry (DSC) measurements showed the high glass transition temperature (T_g) values of PIAnTP and PyIAnTP at 223 and 233 °C, respectively, which was comparable to that of other organic emitters with good thermal stability.[37,38] Such high T_g values indicated that the

https://doi.org/10.1021/acsami.3c09433
ACS Appl. Mater. Interfaces 2023, 15, 47307−47316

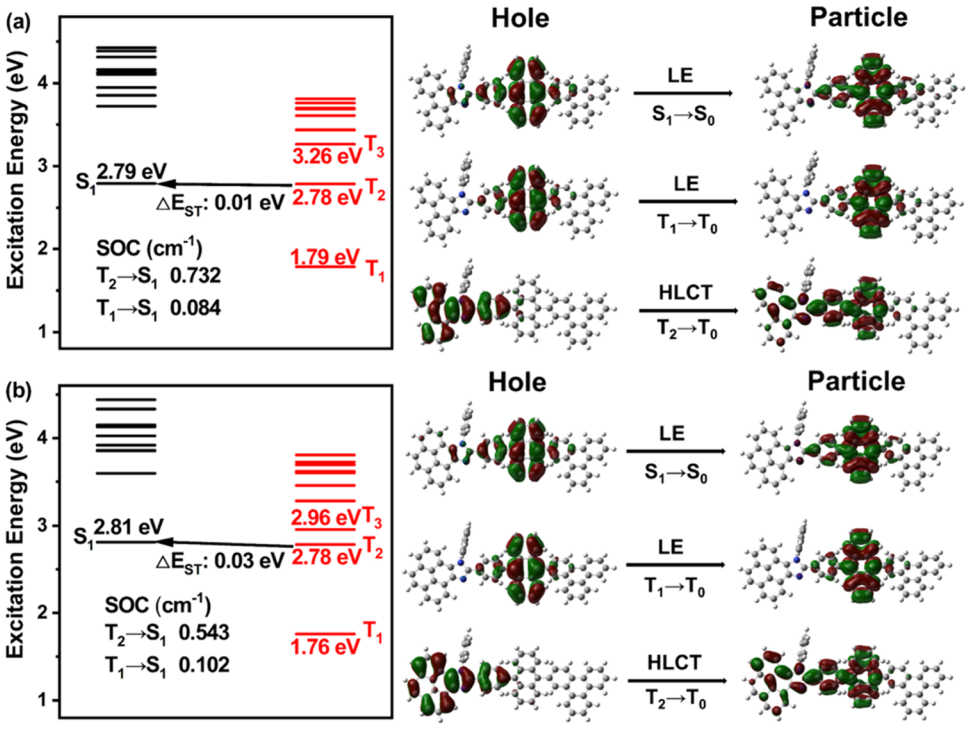

Figure 4. Energy-level diagrams, SOC values between singlets and triplets, and NTO distributions for the $S_1 \rightarrow S_0$, $T_1 \rightarrow T_0$, and $T_2 \rightarrow T_0$ transition PIAnTP (a) and PyIAnTP (b).

solid films of PIAnTP and PyIAnTP can keep an amorphous morphology, which enabled them to function steadily as emitters in organic electronic devices by a vacuum thermal deposition process. We further used XRD measurement to investigate the amorphous morphology of PIAnTP and PyIAnTP. As shown in Figure S3 (Supporting Information), no diffraction peak appeared in the XRD patterns. Furthermore, the electrochemical measurements were carried out by the cyclic voltammetry (CV) method (Figure 2b and Table 1). PIAnTP and PyIAnTP possessed quasi-reversible redox behavior, which indicated good electrochemical stabilities. The onset oxidation potential and reduction potential of PIAnTP and PyIAnTP were found to be 0.90/−2.11 and 0.80/−2.09 eV, respectively, and the calculated HOMO/LUMO energy levels were −5.48/−2.62 and −5.38/−2.64 eV, respectively (Figure S4, Supporting Information). The band gaps of PIAnTP and PyIAnTP were found to be 2.86 and 2.74 eV, respectively, proving that PIAnTP was a better candidate as a potential blue material.

Single-Crystal Analysis. The single crystals of PIAnTP and PyIAnTP were obtained by a temperature-gradient sublimation method and examined by X-ray crystallographic analysis. The two molecules exhibited highly twisted geometry features (Figure 3). For the PIAnTP molecule, the dihedral angles between the anthracene and neighboring decorations were 66.55 and 82.85°, respectively. Larger dihedral angles of 80.90 and 89.15° were observed in the PyIAnTP crystal. The twisted conformation of the molecule can effectively inhibit the close packing of adjacent molecules and decrease the conjugation degree to achieve blue light emission. As a result, no obvious intermolecular $\pi-\pi$ interactions were observed in the PIAnTP and PyIAnTP crystals. The multiple intermolecular C−H···π interactions with bond distances of 2.646−2.844 Å for PIAnTP and 2.654−2.877 Å for PyIAnTP as well as strong intermolecular H-bonds with a short distance of 2.491 Å for PIAnTP were found in crystals. These abundant supramolecular interactions can effectively rigidify molecular structures to suppress the structural vibration, which was in favor of a high PLQY and a narrow FWHM.

Theoretical Calculation. Density functional theory (DFT) was carried out to assess the molecular configurations and HOMO/LUMO distributions of PIAnTP and PyIAnTP. As depicted in Figure S5 (Supporting Information), both compounds showed highly twisted configurations with large twisting angles of 77−81° between anthracene and the neighboring moieties, not only preventing intermolecular $\pi-\pi$ stacking to guarantee blue emissions but also weakened intermolecular interactions in the aggregated state. Meanwhile, the LUMO of PIAnTP and PyIAnTP were fully delocalized on the anthracene moiety with negligible contribution of phenyl rings. Specifically, the HOMO of PIAnTP was mainly located at the anthracene group with some delocalized electron clouds on the PPI group. For PyIAnTP, the HOMO was mainly distributed over the PyI unit with an extension to the adjacent anthracene group due to the stronger donor strength of PyI. Obviously, both molecules exhibited partially overlapped HOMO and LUMO distribution modes, which was propitious for the high fluorescence efficiency and effective transport of carriers.

The natural transition orbital (NTO) distributions were investigated to describe the character of excited states (Figure 4). The S_1 and T_1 states of PIAnTP and PyIAnTP are similar and showed typical LE-like characteristics with "hole" and "particle" concentrating on the anthracene moiety, which was beneficial to improve the PLQY. In comparison, the "hole" of higher triplet energy levels (T_2) states are completely distributed over the PPI/PyI units, while the "particle" was totally delocalized to the PPI/PyI and anthracene fragments. The large proportion overlaps with a partial separation of the "hole" and "particle" wave functions, revealing the HLCT

https://doi.org/10.1021/acsami.3c09433
ACS Appl. Mater. Interfaces 2023, 15, 47307−47316

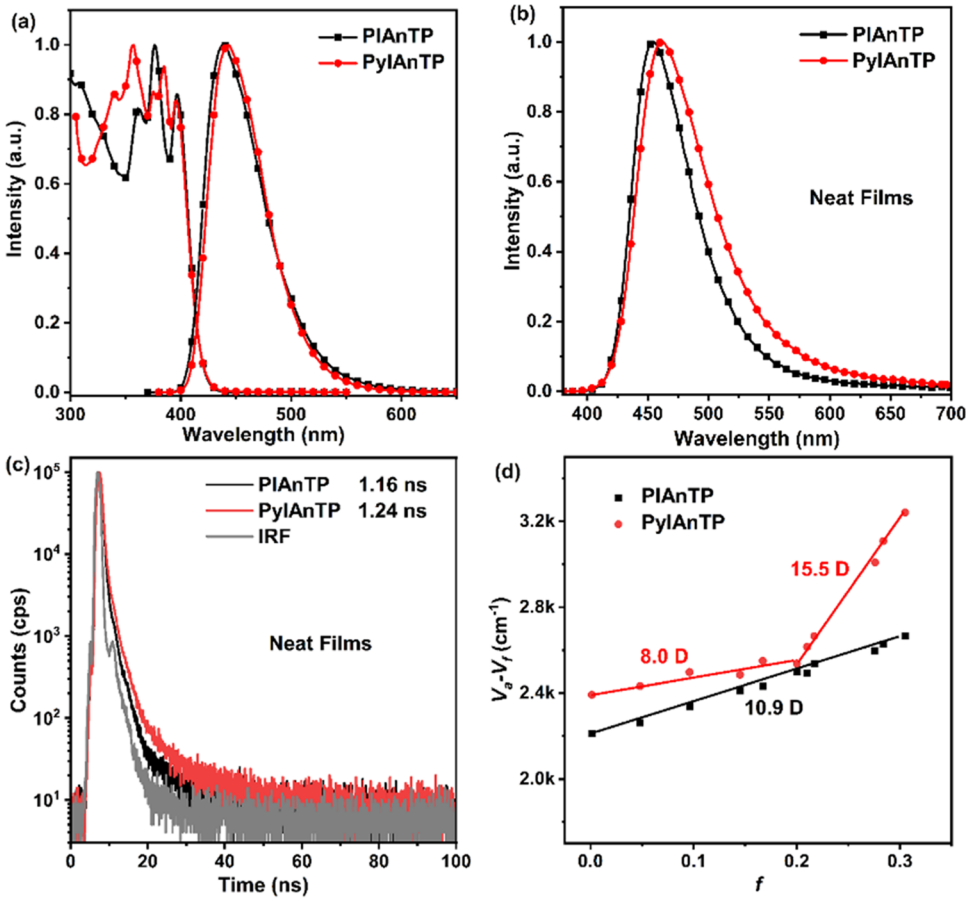

Figure 5. (a) UV−vis and PL spectra of PIAnTP and PyIAnTP in THF solution (10^{-5} M). (b) PL spectra of PIAnTP and PyIAnTP in neat films. (c) Transient PL decay spectra of PIAnTP and PyIAnTP in neat films. (d) Solvatochromic Lippert−Mataga models of PIAnTP and PyIAnTP with the Stokes shift.

characters of the T_2 states for PIAnTP and PyIAnTP. Furthermore, the singlet and triplet energy-level diagrams of two molecules were calculated. Obviously, the energy gaps between S_1 and T_1 are as large as 1.00 and 1.05 eV for PIAnTP and PyIAnTP, which hindered the RISC process from T_1 to S_1 through the TADF process. Nevertheless, the large energy gaps between T_2 and T_1 energy levels of 0.99 and 1.02 eV for PIAnTP and PyIAnTP can be found, indicating that the internal conversion (IC) process from T_2 to T_1 will be largely suppressed. Meanwhile, the energy-level splits between S_1 and T_2 (0.01 and 0.03 eV) were significantly reduced. We further calculated the spin−orbit coupling (SOC) matrix elements using the ORCA program. The SOC values between high-lying T_2 and S_1 (0.732 and 0.543 cm^{-1}) are also larger than that of the T_1 and S_1 (0.084 and 0.102 cm^{-1}), which provided a possibly "hot exciton" channel for the hRISC process from T_2 to S_1 to improve EUE in OLEDs.

Photophysical Properties. The photophysical features of PIAnTP and PyIAnTP consisting of UV−vis absorption and photoluminescence (PL) spectra were analyzed in dilute THF solutions (10^{-5} M) and neat films. As presented in Figure 5 and Table 1, the vibronically structured absorption bands peaking at around 350−400 nm correspond to the π−π^* transition of anthracene. From the onset of the absorption spectra, the optical band gaps (E_g) of PIAnTP and PyIAnTP were estimated to be 2.95 and 2.94 eV, respectively. Compared with the PL spectrum of PIAnTP (peaked at 439 nm), PyIAnTP (peaked at 443 nm) showed a slightly red-shifted emission, which could be ascribed to the extended π-conjugation of PyIAnTP. Meanwhile, the emission peaks in the neat films via physical vapor deposition were also located in the blue region with maximum peaks at 455 and 462 nm for PIAnTP and PyIAnTP, respectively, indicating that the highly twisted conformation of both conformations could effectively reinforce the rigidity to weaken molecular vibrations, thus suppressing nonradiative decays. Therefore, the absolute PLQYs of PIAnTP and PyIAnTP in different polarity solvents were very high (Table S1, Supporting Information). For example, PIAnTP and PyIAnTP showed high PLQYs in THF of 83 and 86%, respectively, demonstrating that the HLCT state is a highly emissive excited state, which was satisfactory for OLED fabrication. In addition, because of the rigid skeleton of PIAnTP and PyIAnTP, the PLQYs in nondoped neat films still can remain as high as 61 and 69%, respectively. Combined with the transient fluorescence lifetime of neat films (Figure 5c), the radiative transition rates (k_rs) and nonradiative transition rates (k_{nr}s) were determined to be 5.26×10^8 and 3.36×10^8 s^{-1} for PIAnTP and 5.56×10^8 and 2.50×10^8 s^{-1} for PyIAnTP, respectively, reflecting that both emitters are potential candidates for OLED applications.[52] The photophysical features of PIAnTP and PyIAnTP doped in the 3,3-bis(*N*-carbazolyl)-1,1′-biphenyl (mCBP) host were also studied to demonstrate the advantage of the rigid conformation in alleviating the concentration caused quenching. The PL spectra and the PLQYs of the mCBP: *x* wt % PIAnTP and PyIAnTP (*x* = 10, 20, 30, 50, 100) doped films are shown

https://doi.org/10.1021/acsami.3c09433
ACS Appl. Mater. Interfaces 2023, 15, 47307−47316

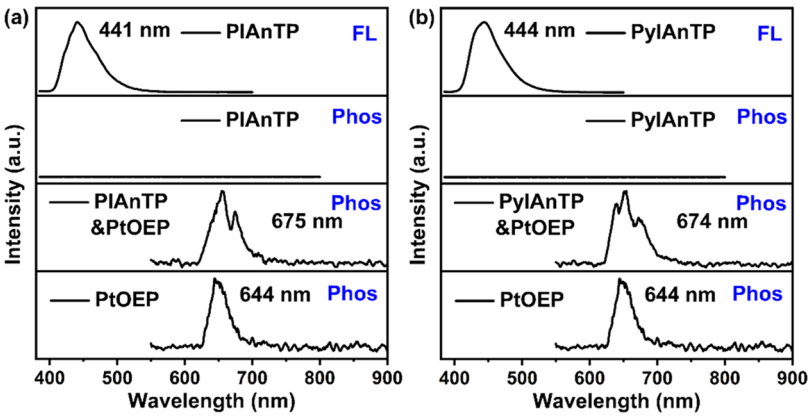

Figure 6. (a) PIAnTP solution fluorescence spectrum and PIAnTP, PIAnTP, and PtOEP and PtOEP phosphorescence spectra at 77 K (5 ms delayed). (b) PyIAnTP solution fluorescence spectrum and PyIAnTP, PyIAnTP, and PtOEP and PtOEP phosphorescence spectra at 77 K (5 ms delayed).

in Figures S8 and S9 and Table S2 (Supporting Information), respectively. Upon increasing the dopant concentration from 10 to 100 wt %, the PL spectra and PLQYs changed little, indicating that aggregation-induced emission quenching and spectral broadening were efficiently suppressed, which were highly desirable for nondoped OLEDs.

To reveal the excited-state properties of PIAnTP and PyIAnTP, the PL emission spectra of the two materials in different solvents with ranged polarities were recorded. As displayed in Figure S11a (Supporting Information), PIAnTP exhibited a tiny red-shift of about 10 nm from hexane (434 nm) to acetonitrile (444 nm), which indicated that the S_1 state of PIAnTP was mainly LE state characteristic, together with a faint CT component. However, the PL spectra of PyIAnTP became broad and displayed a red-shift of 18 nm (Figure S11b, Supporting Information), proving that the S_1 state of PyIAnTP possessed more CT character than PIAnTP, which was in accordance with the theoretical calculations. Furthermore, the Lippert−Mataga solvatochromic model of PIAnTP and PyIAnTP was measured to study the properties of their excited states.[53] As depicted in Figure 5d, PIAnTP presented a good linear relationship with a low excited state dipole moment of 10.9 D, which was the LE-dominated HLCT excited state. PyIAnTP exhibited two-section linear, and the corresponding excited state dipole moments were calculated to be 8.0 and 15.5 D, respectively, indicating the occurrence of nonequivalent hybridization characteristics.[47] The typical HLCT characteristics could also be verified by the transient PL spectra in different polar solvents (Figure S12, Supporting Information). PIAnTP and PyIAnTP both showed mono-exponential attenuation in the nanosecond time scale, indicating that the LE and CT states were integrated into the HLCT state, which was one of the most typical features of the "hot exciton" materials.

We further characterized the fluorescence/phosphorescence spectra at a low-temperature (77 K) matrix to estimate the S_1/T_1 energy levels of these new molecules. As presented in Figure 6, according to the fluorescent emission peak, the energies of the S_1 excited states were estimated to be 2.81 eV for PIAnTP and 2.79 eV for PyIAnTP, respectively. However, no delayed emission spectrum was observed in the 77 K THF solution due to the low population and nonradiative decay energy losses of the T_1 state. Therefore, we used platinum(II) octaethylporphine (PtOEP) with the T_1 of 1.93 eV as the phosphorescent sensitizer to sensitize the T_1 state of PIAnTP and PyIAnTP (Figures S13 and S14, Supporting Information).[54] The sensitized solution of PIAnTP and PyIAnTP showed two clear phosphorescence emissions around 675 and 674 nm, respectively. These new emissions were reasonably ascribed to the emission peaks of the T_1 state, and the calculated T_1 energy levels for PIAnTP and PyIAnTP were 1.84 eV. The ΔE_{ST} values of both molecules were greater than 0.9 eV and the fluorescence decay process exhibited single exponential profiles with lifetimes in the nanosecond scale, which could exclude the TADF process.

Electroluminescence Properties. To investigate whether PIAnTP and PyIAnTP possess bipolar and balanced charge transportability, hole-only devices (HODs) and electron-only devices (EODs) were constructed with the configurations of indium tin oxide (ITO)/1,4,5,8,9,11- hexaazatriphenylenehexacarbonitrile (HATCN) (5 nm)/di-[4-(*N*,*N*-ditolyl-amino)-phenyl] cyclohexane (TAPC) (10 nm)/PIAnTP or PyIAnTP (80 nm)/TAPC (20 nm)/Al (120 nm) and ITO/1,3,5-tri (phenyl-2-benzimidazolyl) benzene (TPBi) (20 nm)/PIAnTP or PyIAnTP (80 nm)/TPBi (10 nm)/LiF (1 nm)/Al (120 nm), respectively. Herein, TAPC and TPBi were used as buffer layers to prevent electron and hole injection. As shown in Figure S16 (Supporting Information), owing to the larger π-conjugated plane of PyI, the more expansive π-electronic delocalization makes PyIAnTP easier to inject and transport electrons simultaneously. With increasing voltage, the hole mobility and electron mobility of PIAnTP and PyIAnTP increase greatly over a wide range of voltages, indicating that they possess bipolar transporting capacities, which is beneficial for high efficiency and low roll-off in devices.

Accounting for the high efficiencies and excellent thermal stability of PIAnTP and PyIAnTP, the nondoped devices by employing PIAnTP and PyIAnTP neat films as the emitting layers (EMLs) were fabricated to evaluate their EL properties. The optimized device configurations of ITO/HATCN (5 nm)/TAPC (30 nm)/TCTA (10 nm)/PIAnTP or PyIAnTP (20 nm)/TPBi (40 nm)/LiF (1 nm)/Al (120 nm) were fabricated by vacuum evaporation, where ITO and Al were used as the anode and cathode, respectively; HATCN, TAPC, TCTA (tris(4-carbazoyl-9-ylphenyl)amine), and LiF were assigned as the hole-injecting layer, the hole transport layer, the exciton block layer, and electron-injecting layer, respectively. Benefiting from the large E_g and deep HOMO

https://doi.org/10.1021/acsami.3c09433
ACS Appl. Mater. Interfaces 2023, 15, 47307−47316

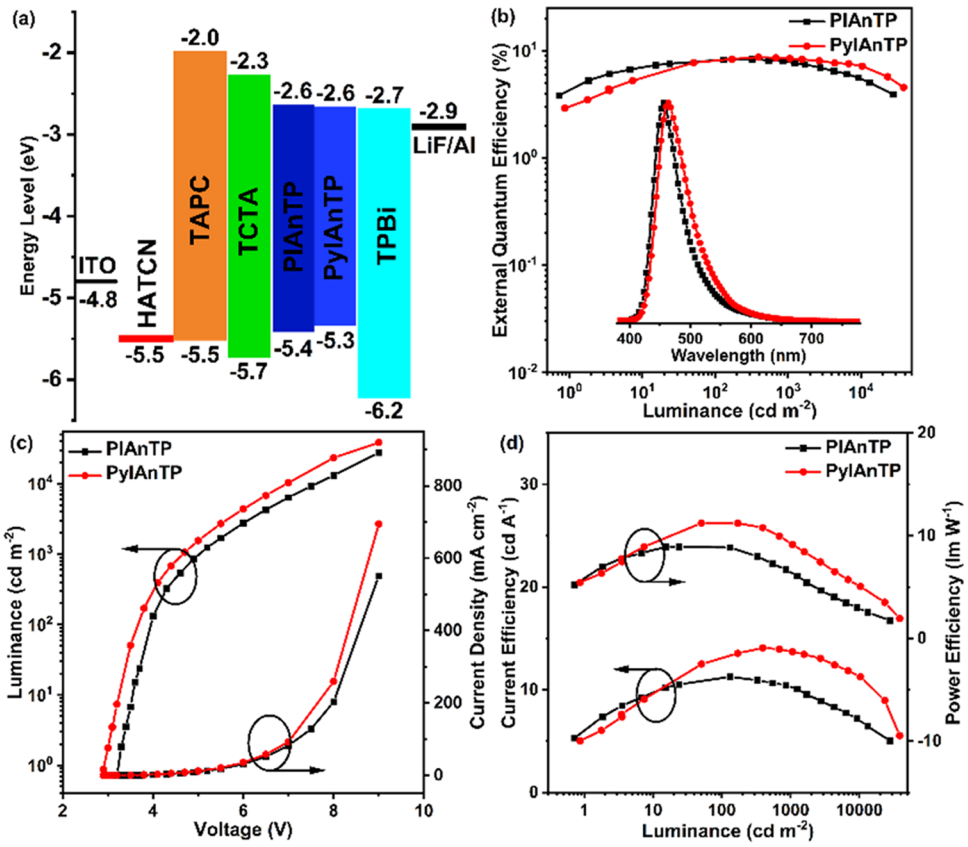

Figure 7. (a) Configuration of the OLED devices. (b) EQE-luminance curves and EL spectra (inset). (c) Luminance−voltage−current density curves. (d) Current efficiency−luminance−power efficiency curves.

Table 2. Summary of EL Performance for the Devices based on PIAnTP and PyIAnTP

device	V_{on}[a] (V)	L_{max}[b] (cd m^{-2})	CE_{max}[c] (cd A^{-1})	PE_{max}[d] (lm W^{-1})	EQE[e] (%) max/1000/10 000 cd m^{-2}	λ_{EL}[f] (nm)	CIE[f] (x, y)	FWHM[f] (nm)
PIAnTP	3.2	27 745	11.28	8.93	8.36/7.87/5.49	456	(0.16, 0.14)	52
PyIAnTP	2.9	38 585	14.09	11.23	8.69/8.48/7.22	464	(0.16, 0.19)	60

[a]Turn-on voltage at 1 cd m^{-2}. [b]Maximum luminance. [c]Maximum current efficiency. [d]Maximum power efficiency. [e]EQE of maximum/at 1000/10 000 cd m^{-2}. [f]Measured at 6 V.

energy level of TPBi, it was picked as the hole-blocking and electron-transporting layers to confine the excitons in the EML (Figure 7a).

The nondoped devices based on PIAnTP and PyIAnTP both showed low turn-on voltages of 3.2 and 2.9 V, indicating balanced charge injection and transfer. PIAnTP- and PyIAnTP-based OLEDs exhibited blue emission at 456 and 464 nm with the corresponding CIE coordinates of (0.16, 0.14) and (0.16, 0.19), respectively. The PIAnTP-based device possessed a narrower emission band with an FWHM of 52 nm compared with PyIAnTP (60 nm), which might be a result of the shorter conjugation length and stronger molecular rigidity of PIAnTP. The EL spectra coincided well with the fluorescence spectra of the two materials' thin films and were very stable with the voltage increases from 4 to 9 V (Figures S17 and S18, Supporting Information), demonstrating that the luminescence originated from the light-emitting materials and the outstanding spectral stability of the EL process. As summarized in Table 2, both devices achieved excellent EL efficiencies with maximum luminance, current efficiency (CE), power efficiency (PE), and EQE of 27745 cd m^{-2}, 11.28 cd A^{-1}, 8.93 lm W^{-1}, and 8.36% for PIAnTP and 38 585 cd m^{-2}, 14.09 cd A^{-1}, 11.23 lm W^{-1}, and 8.69% for PyIAnTP, respectively. It was especially noteworthy that they also exhibited relatively low-efficiency roll-off values of 5.9 and 2.4%, with EQE values remaining at 7.87% for PIAnTP and 8.48% for PyIAnTP at the luminance of 1000 cd m^{-2}. The excellent EL performance of nondoped PIAnTP and PyIAnTP devices was comparable to that of the reported high-efficiency nondoped OLEDs using blue HLCT emitters (Table S3, Supporting Information).

The electrical exciton utilization efficiency was obtained in the range of 46−69% for PIAnTP and 42−63% for PyIAnTP, both of which break through the theoretical limitation of 25% from the spin statistics for conventional fluorescent emitters assuming that the light out-coupling fraction was estimated as 20−30%. This meant that both devices possessed an effective upconversion procedure from triplet exciton to singlet exciton in the EL process. In view of the ΔE_{ST}s of 0.97 and 0.95 eV and the absence of a delay component in the transient PL spectra of PIAnTP and PyIAnTP, the TADF process could be easily excluded. In addition, the EL luminance and current density were both in good linearity, demonstrating that the high utilization of excitons seemed not to originate from the

https://doi.org/10.1021/acsami.3c09433
ACS Appl. Mater. Interfaces 2023, 15, 47307−47316

TTA mechanism (Figure S19, Supporting Information). More importantly, the transient EL decay of PIAnTP- and PyIAnTP-based nondoped devices was further explored. The EL intensities of both devices decayed rapidly after removing electron excitation, and a little delayed component was observed with a clear voltage dependence, suggesting that the delayed part was derived from TTA instead of the collision recombination of trapped charges in the emissive layer.[47] As shown in Figure S20 (Supporting Information), the ratios of the delayed component caused by the TTA process were calculated to be 5.3 and 6.5% at 4 V for PIAnTP- and PyIAnTP-based devices, respectively. According to previous reports,[22,55−57] the proportions of delayed fluorescence caused by the TTA mechanism were further estimated as 2.4−3.7% (=46−69% × 5.3%) and 2.7−4.1% (=42−63% × 6.5%) for PIAnTP and PyIAnTP, respectively, indicating that the contribution of TTA process was not dominant in these nondoped devices. Combining the results of the computational simulations and the analysis of the photophysical properties, the excellent EL performance of PIAnTP and PyIAnTP could be attributed to the "hot exciton" channel for the hRISC process from T_2 to S_1. The fast hRISC process and the inhibited intersystem crossing (IC) process of $T_2 \rightarrow T_1$ were conducive to the much lower concentration of triplet excitons, which can effectively suppress the exciton annihilation, resulting in low-efficiency roll-off at high brightness for a nondoped device. In addition, the imidazole chromophores generally exhibit intrinsic bipolar properties derived from two nitrogen atoms with different bonding modes, which is also beneficial to the balanced charge transportability and relatively low-efficiency roll-off. Therefore, the "hot exciton" material is a promising choice for achieving blue emitters with high-efficiency and low-efficiency roll-offs.

CONCLUSIONS

In conclusion, two blue fluorescent materials, PIAnTP, and PyIAnTP, have been successfully synthesized and characterized. Triphenylene was first introduced to construct blue emitters as the electron acceptor owing to its rigid large-coplanar-conjugated nature, relatively weak electron-withdrawing capacity, and outstanding PL and EL characteristics. The large rigid planar structures and multiple supramolecular interactions in PIAnTP and PyIAnTP enable them to exhibit narrowband blue emissions with relatively high PLQYs. Theoretical simulation and experimental investigations reveal the HLCT characteristic of these molecules, which can achieve the RISC process mainly via a "hot exciton" channel. The PIAnTP- and PyIAnTP-based nondoped OLEDs display pure blue emission with CIE coordinates of (0.16, 0.14) and (0.16, 0.19), maximum luminance of 27 745 and 38 585 cd m^{-2}, and maximum EQE of 8.36 and 8.69%, respectively. More interestingly, both devices had very small efficiency roll-offs of 5.9 and 2.4% at 1000 cd m^{-2} for PIAnTP and PyIAnTP, respectively. It is anticipated that this work will open a new approach for developing high-efficiency "hot exciton" blue materials with narrowband emission by using TP as a promising functional group, which is of vital significance to extend the color gamut beyond the conventional fluorescent.

EXPERIMENTAL SECTION

All detailed experimental procedures for the synthesis and characterization, fabrication, and measurement of OLEDs, and characterization of this work are in the Supporting Information.

ASSOCIATED CONTENT

Supporting Information

The Supporting Information is available free of charge at https: The Supporting Information is available free of charge at https://pubs.acs.org/doi/10.1021/acsami.3c09433.

Experimental details including experimental procedures; synthesis and characterization; thermal properties and electrochemical properties; theoretical calculation; photophysical properties; and electroluminescence properties of the OLEDs (PDF)

PIAnTP (CIF)

PyIAnTP (CIF)

AUTHOR INFORMATION

Corresponding Author

Ping Lu − *State Key Laboratory of Supramolecular Structure and Materials, Department of Chemistry, Jilin University, Changchun 130012, P. R. China;* orcid.org/0000-0001-9144-3488; Email: lup@jlu.edu.cn; Fax: +86 431 85193421

Authors

Futong Liu − *State Key Laboratory of Supramolecular Structure and Materials, Department of Chemistry, Jilin University, Changchun 130012, P. R. China*

Gongyi Cao − *State Key Laboratory of Supramolecular Structure and Materials, Department of Chemistry, Jilin University, Changchun 130012, P. R. China*

Zijun Feng − *State Key Laboratory of Supramolecular Structure and Materials, Department of Chemistry, Jilin University, Changchun 130012, P. R. China*

Zhuang Cheng − *State Key Laboratory of Supramolecular Structure and Materials, Department of Chemistry, Jilin University, Changchun 130012, P. R. China*

Yan Yan − *State Key Laboratory of Supramolecular Structure and Materials, Department of Chemistry, Jilin University, Changchun 130012, P. R. China*

Yangze Xu − *State Key Laboratory of Supramolecular Structure and Materials, Department of Chemistry, Jilin University, Changchun 130012, P. R. China*

Yixuan Jiang − *State Key Laboratory of Supramolecular Structure and Materials, Department of Chemistry, Jilin University, Changchun 130012, P. R. China*

Yulei Chang − *State Key Laboratory of Luminescence and Applications, Changchun Institute of Optics, Fine Mechanics and Physics, Chinese Academy of Sciences, Changchun 130033, P. R. China;* orcid.org/0000-0001-7223-1797

Ying Lv − *State Key Laboratory of Luminescence and Applications, Changchun Institute of Optics, Fine Mechanics and Physics, Chinese Academy of Sciences, Changchun 130033, P. R. China;* orcid.org/0000-0003-1649-5258

Complete contact information is available at: https://pubs.acs.org/10.1021/acsami.3c09433

Notes

The authors declare no competing financial interest.

ACKNOWLEDGMENTS

This research is supported by the National Natural Science Foundation of China (22075100), the Jilin Provincial Science and Technology Department (20220201082GX), the State Key Laboratory of Luminescence, Applications (SKLA-2020-

01), the China Postdoctoral Science Foundation (2022TQ0111, 2023M731267), and the Changsha Automobile Innovation Research Institute.

REFERENCES

(1) Tang, C. W.; VanSlyke, S. A. Organic Electroluminescent Diodes. *Appl. Phys. Lett.* **1987**, *51*, 913−915.
(2) Kido, J.; Kimura, M.; Nagai, K. Multilayer White Light-Emitting Organic Electroluminescent Device. *Science* **1995**, *267*, 1332−1334.
(3) Friend, R. H.; Gymer, R. W.; Holmes, A. B.; Burroughes, J. H.; Marks, R. N.; Taliani, C.; Bradley, D. D. C.; Dos Santos, D. A.; Bredas, J. L.; Logdlund, M.; Salaneck, W. R. Electroluminescence in Conjugated Polymers. *Nature* **1999**, *397*, 121−128.
(4) Uoyama, H.; Goushi, K.; Shizu, K.; Nomura, H.; Adachi, C. Highly Efficient Organic Light-Emitting Diodes from Delayed Fluorescence. *Nature* **2012**, *492*, 234−238.
(5) Reineke, S.; Lindner, F.; Schwartz, G.; Seidler, N.; Walzer, K.; Lüssem, B.; Leo, K. White Organic Light-Emitting Diodes with Fluorescent Tube Efficiency. *Nature* **2009**, *459*, 234−238.
(6) Zhu, M.; Yang, C. Blue Fluorescent Emitters: Design Tactics and Applications in Organic Light-Emitting Diodes. *Chem. Soc. Rev.* **2013**, *42*, 4963−4976.
(7) Im, Y.; Byun, S. Y.; Kim, J. H.; Lee, D. R.; Oh, C. S.; Yook, K. S.; Lee, J. Y. Recent Progress in High-Efficiency Blue-Light-Emitting Materials for Organic Light-Emitting Diodes. *Adv. Funct. Mater.* **2017**, *27*, No. 1603007.
(8) Baldo, M. A.; O'Brien, D. F.; You, Y.; Shoustikov, A.; Sibley, S.; Thompson, M. E.; Forrest, S. R. Highly Efficient Phosphorescent Emission from Organic Electroluminescent Devices. *Nature* **1998**, *395*, 151−154.
(9) Ma, Y.; Zhang, H.; Shen, J.; Che, C. Electroluminescence from Triplet Metal−Ligand Charge-Transfer Excited State of Transition Metal Complexes. *Synth. Met.* **1998**, *94*, 245−248.
(10) Tao, Y.; Yang, C.; Qin, J. Organic Host Materials for Phosphorescent Organic Light-Emitting Diodes. *Chem. Soc. Rev.* **2011**, *40*, 2943−2970.
(11) Zhang, Q.; Li, J.; Shizu, K.; Huang, S.; Hirata, S.; Miyazaki, H.; Adachi, C. Design of Efficient Thermally Activated Delayed Fluorescence Materials for Pure Blue Organic Light Emitting Diodes. *J. Am. Chem. Soc.* **2012**, *134*, 14706−14709.
(12) Zhang, Q.; Li, B.; Huang, S.; Nomura, H.; Tanaka, H.; Adachi, C. Efficient Blue Organic Light-Emitting Diodes Employing Thermally Activated Delayed Fluorescence. *Nat. Photonics* **2014**, *8*, 326−332.
(13) Kaji, H.; Suzuki, H.; Fukushima, T.; Shizu, K.; Suzuki, K.; Kubo, S.; Komino, T.; Oiwa, H.; Suzuki, F.; Wakamiya, A.; Murata, Y.; Adachi, C. Purely Organic Electroluminescent Material Realizing 100% Conversion from Electricity to Light. *Nat. Commun.* **2015**, *6*, No. 8476.
(14) Wada, Y.; Nakagawa, H.; Matsumoto, S.; Wakisaka, Y.; Kaji, H. Organic Light Emitters Exhibiting very Fast Reverse Intersystem Crossing. *Nat. Photonics* **2020**, *14*, 643−649.
(15) Luo, Y.; Li, S.; Zhao, Y.; Li, C.; Pang, Z.; Huang, Y.; Yang, M.; Zhou, L.; Zheng, X.; Pu, X.; Lu, Z. An Ultraviolet Thermally Activated Delayed Fluorescence OLED with Total External Quantum Efficiency over 9. *Adv. Mater.* **2020**, *32*, No. e2001248.
(16) Vázquez, R. J.; Yun, J. H.; Muthike, A. K.; Howell, M.; Kim, H.; Madu, I. K.; Kim, T.; Zimmerman, P.; Lee, J. Y.; Iii, T. G. New Direct Approach for Determining the Reverse Intersystem Crossing Rate in Organic Thermally Activated Delayed Fluorescent (TADF) Emitters. *J. Am. Chem. Soc.* **2020**, *142*, 8074−8079.
(17) Li, W.; Liu, D.; Shen, F.; Ma, D.; Wang, Z.; Feng, T.; Xu, Y.; Yang, B.; Ma, Y. A Twisting Donor-Acceptor Molecule with an Intercrossed Excited State for Highly Efficient, Deep-Blue Electroluminescence. *Adv. Funct. Mater.* **2012**, *22*, 2797−2803.
(18) Li, W.; Pan, Y.; Xiao, R.; Peng, Q.; Zhang, S.; Ma, D.; Li, F.; Shen, F.; Wang, Y.; Yang, B.; Ma, Y. Employing ∼ 100% Excitons in OLEDs by Utilizing a Fluorescent Molecule with Hybridized Local and Charge-Transfer Excited State. *Adv. Funct. Mater.* **2014**, *24*, 1609−1614.
(19) Ouyang, X.; Li, X. L.; Ai, L.; Mi, D.; Ge, Z.; Su, S. J. Novel "Hot Exciton" Blue Fluorophores for High Performance Fluorescent/Phosphorescent Hybrid White Organic Light-Emitting Diodes with Super High Phosphorescent Dopant Concentration and Improved Efficiency Roll-Off. *ACS Appl. Mater. Interfaces* **2015**, *7*, 7869−7877.
(20) Wang, C.; Li, X.; Pan, Y.; Zhang, S.; Yao, L.; Bai, Q.; Li, W.; Lu, P.; Yang, B.; Su, S.; Ma, Y. Highly Efficient Nondoped Green Organic Light-Emitting Diodes with Combination of High Photoluminescence and High Exciton Utilization. *ACS Appl. Mater. Interfaces* **2016**, *8*, 3041−3049.
(21) Xu, Y.; Liang, X.; Zhou, X.; Yuan, P.; Zhou, J.; Wang, C.; Li, B.; Hu, D.; Qiao, X.; Jiang, X.; Liu, L.; Su, S. J.; Ma, D.; Ma, Y. Highly Efficient Blue Fluorescent OLEDs Based on Upper Level Triplet-Singlet Intersystem Crossing. *Adv. Mater.* **2019**, *31*, No. 1807388.
(22) Li, B.; Lou, J.; Zhang, H.; Li, G.; He, X.; Huang, Y.; Zheng, N.; Wang, Z.; Ma, D.; Tang, B. Z. Exciton Recovery" Strategy in Hot Exciton Emitter toward High-Performance Non-Doped Deep-Blue and Host-Sensitized Organic Light-Emitting Diodes. *Adv. Funct. Mater.* **2023**, *33*, No. 2212876, DOI: 10.1002/adfm.202212876.
(23) Im, Y.; Kim, M.; Cho, Y. J.; Seo, J.-A.; Yook, K. S.; Lee, J. Y. Molecular Design Strategy of Organic Thermally Activated Delayed Fluorescence Emitters. *Chem. Mater.* **2017**, *29*, 1946−1963.
(24) Li, X.; Shi, Y.-Z.; Wang, K.; Zhang, M.; Zheng, C.-J.; Sun, D.-M.; Dai, G.-L.; Fan, X.-C.; Wang, D.-Q.; Liu, W.; Li, Y.-Q.; Yu, J.; Ou, X.-M.; Adachi, C.; Zhang, X.-H. Thermally Activated Delayed Fluorescence Carbonyl Derivatives for Organic Light-Emitting Diodes with Extremely Narrow Full Width at Half-Maximum. *ACS Appl. Mater. Interfaces* **2019**, *11*, 13472−13480.
(25) Santoro, F.; Lami, A.; Improta, R.; Bloino, J.; Barone, V. Effective Method for The Computation of Optical Spectra of Large Molecules at Finite Temperature Including the Duschinsky and Herzberg−Teller effect: The Qx Band of Porphyrin as a Case Study. *J. Chem. Phys.* **2008**, *128*, No. 224311.
(26) Hatakeyama, T.; Shiren, K.; Nakajima, K.; Nomura, S.; Nakatsuka, S.; Kinoshita, K.; Ni, J.; Ono, Y.; Ikuta, T. Ultrapure Blue Thermally Activated Delayed Fluorescence Molecules: Efficient HOMO-LUMO Separation by the Multiple Resonance Effect. *Adv. Mater.* **2016**, *28*, 2777−2781.
(27) Kondo, Y.; Yoshiura, K.; Kitera, S.; Nishi, H.; Oda, S.; Gotoh, H.; Sasada, Y.; Yanai, M.; Hatakeyama, T. Narrowband Deep-Blue Organic Light-Emitting Diode Featuring an Organoboron-Based Emitter. *Nat. Photonics* **2019**, *13*, 678−682.
(28) Zhang, Y.; Zhang, D.; Wei, J.; Liu, Z.; Lu, Y.; Duan, L. Multi-Resonance Induced Thermally Activated Delayed Fluorophores for Narrowband Green OLEDs. *Angew. Chem., Int. Ed.* **2019**, *58*, 16912−16917.
(29) Yang, M.; Park, I. S.; Yasuda, T. Full-Color, Narrowband, and High-Efficiency Electroluminescence from Boron and Carbazole Embedded Polycyclic Heteroaromatics. *J. Am. Chem. Soc.* **2020**, *142*, 19468−19472.
(30) Xu, Y.; Li, C.; Li, Z.; Wang, Q.; Cai, X.; Wei, J.; Wang, Y. Constructing Charge-Transfer Excited States Based on Frontier Molecular Orbital Engineering: Narrowband Green Electroluminescence with High Color Purity and Efficiency. *Angew. Chem., Int. Ed.* **2020**, *59*, 17442−17446.
(31) Nagata, M.; Min, H.; Watanabe, E.; Fukumoto, H.; Mizuhata, Y.; Tokitoh, N.; Agou, T.; Yasuda, T. Fused-Nonacyclic Multi-Resonance Delayed Fluorescence Emitter Based on Ladder-Thiaborin Exhibiting Narrowband Sky-Blue Emission with Accelerated Reverse Intersystem Crossing. *Angew. Chem., Int. Ed.* **2021**, *60*, 20280−20285.
(32) Hu, Y. X.; Miao, J.; Hua, T.; Huang, Z.; Qi, Y.; Zou, Y.; Qiu, Y.; Xia, H.; Liu, H.; Cao, X.; Yang, C. Efficient Selenium-Integrated TADF OLEDs with Reduced Roll-Off. *Nat. Photonics* **2022**, *16*, 803−810.
(33) Luo, X. F.; Song, S. Q.; Ni, H. X.; Ma, H.; Yang, D.; Ma, D.; Zheng, Y. X.; Zuo, J. L. Multiple-Resonance-Induced Thermally Activated Delayed Fluorescence Materials Based on Indolo[3,2,1-

jk]carbazole with an Efficient Narrowband Pure-Green Electroluminescence. *Angew. Chem., Int. Ed.* **2022**, *61*, No. e202209984.
(34) Liao, Y. Z.; Strong, V.; Wang, Y.; Li, X.-G.; Wang, X.; Kaner, R. B. Oligotriphenylene Nanofiber Sensors for Detection of Nitro-Based Explosives. *Adv. Funct. Mater.* **2012**, *22*, 726−735.
(35) Yoon, T.; Park, I.; Nguyen, T. P.; Kim, D. Y.; Lee, J.; Shim, J. H.; Choi, H. C. Discovery of Sodium-Doped Triphenylene Superconductors by Searching the Organic Material Database. *Chem. Mater.* **2020**, *32*, 3358−3364.
(36) Wagner, J.; Zimmermann Crocomo, P.; Kochman, M. A.; Kubas, A.; Data, P.; Lindner, M. Modular Nitrogen-Doped Concave Polycyclic Aromatic Hydrocarbons for High-Performance Organic Light-Emitting Diodes with Tunable Emission Mechanisms. *Angew. Chem., Int. Ed.* **2022**, *61*, No. e202202232.
(37) Lv, X.; Sun, M.; Xu, L.; Wang, R.; Zhou, H.; Pan, Y.; Zhang, S.; Sun, Q.; Xue, S.; Yang, W. Highly Efficient Non-doped Blue Fluorescent OLEDs with Low Efficiency Roll-Off based on Hybridized Local and Charge Transfer Excited State Emitters. *Chem. Sci.* **2020**, *11*, 5058−5065.
(38) Lv, X.; Xu, L.; Cang, M.; Wang, R.; Sun, M.; Zhou, H.; Yu, Y.; Sun, Q.; Pan, Y.; Xu, Y.; Hu, D.; Xue, S.; Yang, W. Pure-Blue Fluorescence Molecule for Nondoped Electroluminescence with External Quantum Efficiency Approaching 13%. *CCS Chem.* **2021**, *3*, 2557−2568.
(39) Yu, Y.; Xu, P.; Pan, Y.; Qiao, X.; Ying, L.; Hu, D.; Ma, D.; Ma, Y. Pyrene-Based Emitters with Ultrafast Upper-Level Triplet−Singlet Intersystem Crossing for High-Efficiency, Low Roll-Off Blue Organic Light-Emitting Diode. *Adv. Opt. Mater.* **2023**, *11*, No. 2202217.
(40) Zeng, J.; Qiu, N.; Zhang, J.; Wang, X.; Redshaw, C.; Feng, X.; Lam, J. W. Y.; Zhao, Z.; Tang, B. Z. Y-Shaped Pyrene-Based Aggregation-Induced Emission Blue Emitters for High-Performance OLED Devices. *Adv. Opt. Mater.* **2022**, *10*, No. 2200917.
(41) Li, A.; Li, F.; Chen, Y.; Xie, Y.; Li, X.; Liu, X.; Xu, S.; Xu, W.; Wang, J.; Li, Z. Flexible and Continuous Regulation Promoting Remarkably Emission Enhancement of Planar Triphenylene. *ACS Mater. Lett.* **2022**, *4*, 2151−2158.
(42) Chen, W.; Zhang, H.; Zheng, H.; Li, H.; Guo, F.; Ni, G.; Ma, M.; Shi, C.; Ghadari, R.; Hu, L. Two-Dimensional Triphenylene Cored Hole-Transporting Materials for Efficient Perovskite Solar Cells. *Chem. Commun.* **2020**, *56*, 1879−1882.
(43) Bala, I.; Yang, W.-Y.; Gupta, S. P.; De, J.; Yadav, R. A. K.; Singh, D. P.; Dubey, D. K.; Jou, J.-H.; Douali, R.; Pal, S. K. Room Temperature Discotic Liquid Crystalline Triphenylene-Pentaalkynylbenzene Dyads as an Emitter in Blue OLEDs and Their Charge Transfer Complexes with Ambipolar Charge Transport Behaviour. *J. Mater. Chem. C* **2019**, *7*, 5724−5738.
(44) Lin, H.; Zhao, K.-X.; Jing, M.; Long, X.-H.; Zhao, K.-Q.; Hu, P.; Wang, B.-Q.; Lei, P.; Zeng, Q.-D.; Donnio, B. Synthesis, Self-Assembly and Optical Properties of Some Rigid π-Bridged Triphenylene Dimers. *J. Mater. Chem. C* **2022**, *10*, 14453−14470.
(45) Liu, Y.; Liu, H.; Bai, Q.; Du, C.; Shang, A.; Jiang, D.; Tang, X.; Lu, P. Pyrene[4,5-d]imidazole-Based Derivatives with Hybridized Local and Charge-Transfer State for Highly Efficient Blue and White Organic Light-Emitting Diodes with Low Efficiency Roll-Off. *ACS Appl. Mater. Interfaces* **2020**, *12*, 16715−16725.
(46) Liu, Y.; Man, X.; Bai, Q.; Liu, H.; Liu, P.; Fu, Y.; Hu, D.; Lu, P.; Ma, Y. Highly Efficient Blue Organic Light-Emitting Diode Based on a Pyrene[4,5-d]Imidazole-Pyrene Molecule. *CCS Chem.* **2022**, *4*, 214−227.
(47) Du, C.; Lu, T.; Cheng, Z.; Chang, Y.; Liu, H.; Wang, J.; Wan, L.; Lv, Y.; Lu, P. Rational Molecular Design of Phenanthroimidazole-based Fluorescent Materials Towards High-Efficiency Non-Doped Deep Blue OLEDs. *J. Mater. Chem. C* **2022**, *10*, 14186−14193.
(48) Tang, X.; Bai, Q.; Shan, T.; Li, J.; Gao, Y.; Liu, F.; Liu, H.; Peng, Q.; Yang, B.; Li, F.; Lu, P. Efficient Nondoped Blue Fluorescent Organic Light-Emitting Diodes (OLEDs) with a High External Quantum Efficiency of 9.4% @ 1000 cd m-2 Based on Phenanthroimidazole−Anthracene Derivative. *Adv. Funct. Mater.* **2018**, *28*, No. 1705813.
(49) Liu, F.; Man, X.; Liu, H.; Min, J.; Zhao, S.; Min, W.; Gao, L.; Jin, H.; Lu, P. Highly Efficient Nondoped Blue Organic Light-Emitting Diodes With High Brightness and Negligible Efficiency Roll-Off based on Anthracene-Triazine Derivatives. *J. Mater. Chem. C* **2019**, *7*, 14881−14888.
(50) Liu, F.; Liu, H.; Tang, X.; Ren, S.; He, X.; Li, J.; Du, C.; Feng, Z.; Lu, P. Novel Blue Fluorescent Materials for High-Performance Nondoped Blue OLEDs and Hybrid Pure White OLEDs with Ultrahigh Color Rendering Index. *Nano Energy* **2020**, *68*, No. 104325.
(51) Liu, F.; Cheng, Z.; Wan, L.; Gao, L.; Yan, Z.; Hu, D.; Ying, L.; Lu, P.; Ma, Y. Anthracene-Based Emitters for Highly Efficient Deep Blue Organic Light-Emitting Diodes with Narrow Emission Spectrum. *Chem. Eng. J.* **2021**, *426*, No. 131351.
(52) Liu, F.; Tan, Y.; Liu, H.; Tang, X.; Gao, L.; Du, C.; Min, J.; Jin, H.; Lu, P. High-Efficiency Near-Infrared Fluorescent Organic Light-Emitting Diodes with Small efficiency Roll-off Based on AIE-active Phenanthro[9,10-d]imidazole Derivatives. *J. Mater. Chem. C* **2020**, *8*, 6883−6890.
(53) Grabowski, Z. R.; Rotkiewicz, K.; Rettig, W. Structural Changes Accompanying Intramolecular Electron Transfer: Focus on Twisted Intramolecular Charge-Transfer States and Structures. *Chem. Rev.* **2003**, *103*, 3899−4032.
(54) Ponterini, G.; Serpone, N.; Bergkamp, M. A.; Netzel, T. L. Comparison of Radiationless Decay Processes in Osmium and Platinum Porphyrins. *J. Am. Chem. Soc.* **1983**, *105*, 4639−4645.
(55) Chen, C. H.; Tierce, N. T.; Leung, M. K.; Chiu, T. L.; Lin, C. F.; Bardeen, C. J.; Lee, J. H. Efficient Triplet-Triplet Annihilation Upconversion in an Electroluminescence Device with a Fluorescent Sensitizer and a Triplet-Diffusion Singlet-Blocking Layer. *Adv. Mater.* **2018**, *30*, No. e1804850.
(56) Guo, R.; Liu, W.; Ying, S.; Xu, Y.; Wen, Y.; Wang, Y.; Hu, D.; Qiao, X.; Yang, B.; Ma, D.; Wang, L. Exceptionally Efficient Deep Blue Anthracene-Based Luminogens: Design, Synthesis, Photophysical, and Electroluminescent Mechanisms. *Sci. Bull.* **2021**, *66*, 2090−2098.
(57) Lim, H.; Woo, S. J.; Ha, Y. H.; Kim, Y. H.; Kim, J. J. Breaking the Efficiency Limit of Deep-Blue Fluorescent OLEDs Based on Anthracene Derivatives. *Adv. Mater.* **2022**, *34*, No. e2100161.

https://doi.org/10.1021/acsami.3c09433
ACS Appl. Mater. Interfaces 2023, 15, 47307−47316